Vibronic coupling in indole: II. Investigation of the ^1L_a–^1L_b interaction using rotationally resolved electronic spectroscopy†

Jochen Küpper,*[abc] David W. Pratt,*[a] W. Leo Meerts,*[d] Christian Brand,[b] Jörg Tatchen[ae] and Michael Schmitt*[b]

Received 26th January 2010, Accepted 20th March 2010
First published as an Advance Article on the web 19th April 2010
DOI: 10.1039/c001778g

High-resolution electronic spectra of indole (C_8H_7N) and their detailed analysis are reported. Thirteen low-lying vibronic bands—from the electronic origin transition at 35 231.4 cm^{-1} up to 1000 cm^{-1} above—are recorded with rotational resolution. Besides inertial parameters and inertial defects these spectra yield detailed information, for each individual band, on the transition-dipole-moment orientations in the molecular inertial frame as well as on the reorientation of that inertial frame upon electronic excitation. The natural lifetimes of the individual vibronic states have also been determined. Strongly varying orientations of the transition-dipole-moments, unexpected positive inertial defects, and decreasing lifetimes, which are only partly related to increased excitation energy, are observed. These results are clear indications of the interaction of the two lowest electronically excited singlet states (^1L_b and ^1L_a). Our experimental findings are strongly supported by, and in excellent agreement with, the theoretical description of the interaction of the two electronic states described in the preceding paper. These results provide clear evidence for strong vibronic coupling of the two electronic states ^1L_b and ^1L_a and for the energetic location of the ^1L_a-state more than 1000 cm^{-1} above the ^1L_b vibrationless state.

1. Introduction

Indole is the chromophore of the amino acid tryptophan (Trp), whose intrinsic emission properties are used in many fluorescence experiments on proteins.[1] As a result, the molecule has prompted considerable experimental and theoretical interest. (For an overview of the theoretical studies see the previous paper[2] and references therein). Experimentally, the ground-state structure was investigated by microwave spectroscopy[3,4] and the lowest-frequency vibronic band, the ^1L_b origin, has also been observed by rotationally resolved laser spectroscopy.[5,6] These studies yield detailed structural information for the ground electronic state and the first excited electronic state. The dipole moments of indole in its ground and first excited electronic states were determined to be 1.963 D and 1.856 D, respectively.[7]

Following Platt,[8] the lowest electronically excited states of cata-concatenated hydrocarbons are labeled ^1L_b and ^1L_a. This nomenclature is typically also applied to unsymmetrical molecules, such as the heterocyclic indole. Due to its low molecular symmetry, the two states belong to the same representation and can therefore only be distinguished by their spectral signatures. Moreover, the states are assumed to be close in energy and, therefore, are strongly coupled. The ^1L_b and ^1L_a states can be distinguished by their electronic properties. Generally, the electronic transition dipole moment vectors (TDM) for excitation from the electronic ground state to the two states are oriented differently in the molecular frame; typically, they are nearly orthogonal to each other.[9] Moreover, the ^1L_a state is very polar and, therefore, its energy depends strongly on the polarity of its solvent environment, whereas this is typically not the case for ^1L_b.

Vibronic transitions to the lowest electronically excited states and the accompanying dynamics have been extensively studied. The ^1L_b origin transition was determined to lie at 35 323 cm^{-1} and its fluorescence lifetime is 17.5 ns.[10] The ^3L_a origin transition was observed at 24 933 cm^{-1} for indole embedded in cryogenic matrices.[11,12] An analysis of the vibrational levels in the electronic ground and first excited state (^1L_b) revealed a clear correspondence of ground and excited vibrational modes up to 718 cm^{-1}, whereas for higher energies this was not true.[13] The fluorescence lifetimes of many vibronic bands up to 919 cm^{-1} were determined and showed a mostly gradual decrease from 16.4 ns for the origin transition down to 11 ns for the highest bands.[13]

The electronic TDM direction θ is defined in Fig. 1. This TDM angle was previously determined to be $+42(5)^\circ$ and $-46(5)^\circ$ for ^1L_b and ^1L_a for indole embedded in stretched

[a] *University of Pittsburgh, Department of Chemistry, Pittsburgh, PA 15260, USA. E-mail: pratt@pitt.edu*
[b] *Heinrich-Heine-Universität, Institut für Physikalische Chemie I, 40225 Düsseldorf, Germany. E-mail: mschmitt@uni-duesseldorf.de*
[c] *Fritz-Haber-Institut der Max-Planck-Gesellschaft, 14195 Berlin, Germany. E-mail: jochen@fhi-berlin.mpg.de*
[d] *Radboud University Nijmegen, Institute for Molecules and Materials, Heyendaalseweg 135, NL-6525 AJ Nijmegen, The Netherlands. E-mail: leo.meerts@science.ru.nl*
[e] *Chemical Physics Department, Weizmann Institute of Science, 76100 Rehovot, Israel*

† Electronic supplementary information (ESI) available: The rovibronic spectra of the vibronic bands at 480, 539, 718, 720, 737, 909, 910 and 968 cm^{-1} above the electronic origin at 35 231.4 cm^{-1}. See DOI: 10.1039/c001778g

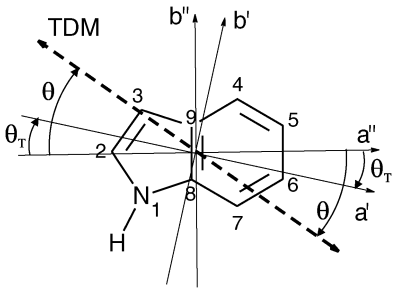

Fig. 1 Structure and definition of inertial axes, transition-dipole-moment orientation θ and inertial-axis reorientation angle θ_T.

polyethylene films, respectively.[14] From rotationally resolved spectroscopy, the ^1L_b TDM orientation was determined to be $|\theta| = 38.3(2)^\circ$.[6] From two-photon excitation spectroscopy of gas-phase indole, the ^1L_a origin was assigned just 450 cm^{-1} above the ^1L_b electronic origin transition.[15] Later, a detailed vibronic analysis lead to the conclusion that all bands up to 1000 cm^{-1} above the origin transition belong to the ^1L_b electronic state.[16] This was confirmed by polarized fluorescence excitation and dispersed fluorescence spectra of indole in solid argon, which suggested an energy of the ^1L_a state 1400 cm^{-1} above the ^1L_b state.[17]

The solvochromatic response of the two electronically excited states is expected to be quite different. Whereas the ^1L_b state behaves similarly to the ground electronic state, the ^1L_a energy depends strongly on the solvent. These effects have been probed using microsolvation in van-der-Waals clusters using vibrationally[10,18–21] and rotationally resolved spectroscopy.[22–24] From Stark effect measurements the dipole moment of indole-water in its ground and first excited electronic state was determined and a significant change of the water molecules' orientation upon excitation was observed.[7]

In the preceding article (paper I), vibronic coupling between the two lowest singlet states of indole was investigated theoretically. This coupling makes the experimental identification of the exact location of the ^1L_a origin difficult. In this second, experimental, paper, we present rotationally resolved spectra of a number of vibronic bands up to 989 cm^{-1} above the ^1L_b origin transition. From these spectra, we extract detailed structural information (rotational constants, inertial defects, inertial axis reorientation angles), TDM angles of the individual vibronic bands, including their signs, and natural lifetimes of the respective excited vibronic states. These data serve as a benchmark for the theoretical description given in paper I and lead to a clear description of the first electronically excited singlet states of indole.

2. Experimental methods

The experiments were performed in two stages; initial measurements were performed at the University of Pittsburgh, later experiments were performed at the Heinrich-Heine-University in Düsseldorf, in both cases using similar experimental setups that have been described elsewhere.[25,26] In brief, indole was heated to 100 °C, seeded in 300–500 mbar of argon, and expanded into vacuum. The beam was confined by skimmers, resulting in Doppler broadening of individual rotational lines smaller than 20 MHz full-width-at-half-maximum (FWHM), in a differentially pumped vacuum system. The molecular beam was crossed at right angles by UV radiation near 280 nm from frequency-doubled narrow-linewidth (FWHM < 1 MHz) continuous-wave ring-dye-lasers (Spectra Physics 380D or Sirah Matisse DS) and the integrated laser-induced fluorescence was collected using a lens system onto a photomultiplier tube. The relative frequency was determined by comparison to a quasi-confocal Fabry–Perot interferometer and the absolute frequency was determined by simultaneously recording the iodine absorption spectrum and successive comparison to the tabulated transition frequencies.[27]

3. Theoretical methods

3.1 Evolutionary strategies

The rovibronic spectra were fitted to an asymmetric rotor Hamiltonian with axis reorientation using a derandomized (DR) evolutionary strategy (ES).[28] The results are in agreement with the subset of previously obtained parameters using an assigned fit for the inertial parameters and a conventional contour fit for the TDM and axis reorientation angles.[29]

We used a special implementation of the de-randomized ES which is abbreviated in the following as DR2.[30] For many applications, the DR2 algorithm has been shown to be superior[31] to the genetic algorithm (GA) used in automated spectral assignments, so far.[32–34] Both GA and ES are inspired by evolutionary processes in nature which are based on reproduction, mutation, and selection. The quality of each solution is analyzed by means of a fitness function,[32,35] While the GA tries to find a solution in the parameter space by combining information from a set of randomly generated solutions with the aim of creating better ones, the DR2 algorithm additionally can analyze and use the information in which direction the fitness increases. In its initial step, the DR2 algorithm randomly generates some trial solutions each consisting of the complete parameter set necessary to describe the spectrum. The fitness of the offspring is compared to that of the parents and the best become themselves parent(s) for the next generation. If for some parameter a parent has evolved in the same direction for several generations, so that their correlation in this parameter is positive, the most likely solution is assumed to be further in that direction and the next parameter mutation will be larger. Correspondingly, two anticorrelated mutations will lead to a smaller mutation. By discriminating between mutation rates for different parameters, the DR2 algorithm can reliably find the optimal solution within a relatively small number of generations.[28]

When used to fit our spectra, the DR2 algorithm succeeded in obtaining good fits with a smaller population and within fewer generations compared to the genetic algorithm (GA). Although the computation of each generation is more expensive, the total effect is a reduction in the total computation time by a factor of two compared to the GA.[32–34] Since the ES uses the complete spectrum, also parts of the spectrum are included in the calculation of the fitness function which show only small deviations from the rigid rotor intensities (*cf.* subsection 3.2). Therefore, we restricted the calculation of the fitness function

in a first step to regions of the spectrum with rovibronic transitions that show a large dependence upon axis reorientation. These ranges were determined in an interactive manner to include in each fit the maximum number of transitions. The final fits were then performed with the entire spectrum.

3.2 Axis reorientation

For the computation of intensities in rovibronic spectra, the Euler angles, which define the angles between the rotating molecule fixed coordinate system in which the TDM is defined and the space fixed coordinate system of the radiation field, have to be calculated. The approximation of common inertial systems for both electronic states, uses the fact, that the structure of a molecule changes only slightly upon electronic excitation, so that the molecule fixed coordinate systems for the ground and the excited states coincide. Once this approximation becomes invalid, the rotation of the principal axis system upon excitation has to be taken into account. The principal axis system in indole rotates about the *c*-axis and although the angle of rotation is generally small, the effect on the intensities of the rotational transitions can be very pronounced.

For a correct calculation of the intensities, all rotational wave functions of the ground and the excited state should be expressed in a common coordinate system. This can be achieved by transforming the excited state rotational Hamiltonian *via* a rotation of $\vec{J}$ around the *c* axis by an angle θ_T:[36]

$$\begin{aligned} H' = {} & (A' \cos^2\theta_T + B' \sin^2\theta_T) J_a'^2 \\ & + (A' \sin^2\theta_T + B' \cos^2\theta_T) J_b'^2 + C' J_c'^2 \\ & + (A' - B') \sin\theta_T \cos\theta_T (J_a' J_b' + J_b' J_a') \end{aligned} \quad (1)$$

In this way the excited state Hamiltonian is expressed in the coordinate system of the ground state and its eigenfunctions can therefore be given within the same basis set as the ground state functions. It is readily seen that the matrix elements of the transformed effective rotational Hamiltonian given in eqn (1) are the same as those for the rigid rotor Hamiltonian. The cross term $J_aJ_b + J_bJ_a$ however, gives rise to a new matrix element:

$$\langle JK|(J_aJ_b + J_bJ_a)|JK \pm 1\rangle = \tfrac{1}{2}(2K \pm 1)[J(J+1) - K(K \pm 1)]^{\frac{1}{2}} \quad (2)$$

4. Experimental results

Fig. 2 shows the fluorescence excitation spectrum of indole in the region from 0 to 1200 cm^{-1} above the origin at 35 231.4 cm^{-1}. The bands that have been further investigated with rotational resolution are marked with their vibrational excitation wavenumbers in Fig. 2.

The rotationally resolved spectrum of the electronic origin of indole has been presented elsewhere[5,6] and our results are in full agreement with the published data. Here, we discuss the vibronic bands from 316 up to 989 cm^{-1} above the electronic origin at 35 231.4 cm^{-1}. Table 1 summarizes the results of the fit to the Hamiltonian in eqn (1) for each of these bands. The rotational constants of the ground state have been taken from refs. 3 and 4. Table 1 reports the changes of the rotational constant upon electronic excitation,‡ the direction of the TDM θ, the axis reorientation angle θ_T, the excited state lifetime τ (determined from the Lorentzian contribution to the individual Voigt lineshapes), the center frequency $\tilde{\nu}_0$, and the exact frequency shift from the vibrationless origin $\Delta\tilde{\nu}_0$. Figs. 3–6 show representative experimental high-resolution spectra, their simulations, and expanded views of experimental and simulated spectra, of the bands at 316, 379, 454, and 989 cm^{-1} above the electronic origin of indole. The simulations shown in these figures are calculated using the best-fit parameters given in Table 1. Spectra and simulations of all other bands given in Table 1 are presented in the ESI.†

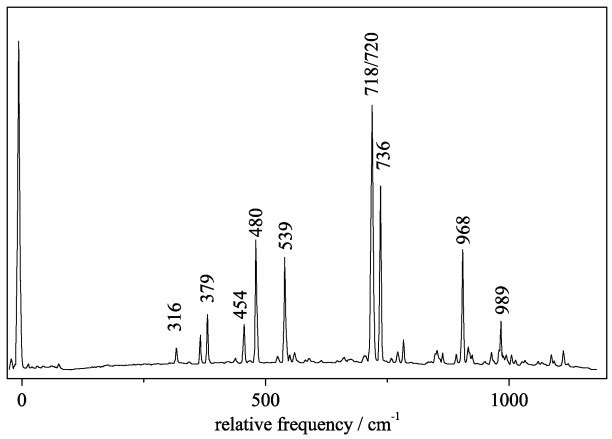

Fig. 2 Electronic excitation spectrum of indole in the region from 0 to 1200 cm^{-1} above the electronic origin at 35231.4 cm^{-1}.

5. Discussion

5.1 Transition-dipole-moment directions

The electronic origin band of indole is classified under the Platt nomenclature as a ^1L_b band. In this band, the TDM makes an angle θ of $\pm 39^\circ$ with the inertial *a*-axis.[6] From a comparison to the values from linear dichroism measurements of "partially oriented" indole molecules in a stretched polyethylene host, the sign of θ can be determined to be positive ($+39^\circ$).[14] The same absolute orientation was obtained from a comparison of the rotationally resolved electronic origin spectra of indole and the van der Waals bound indole-Ar cluster.[24] This value also is consistent with the results of the DFT/MRCI calculations in paper I. Overall, the orientation of the TDM for the ^1L_b state can unambiguously be determined as being positive; see Fig. 1 for a depiction of this angle. From Table 1 it then follows immediately that the

‡ We want to point out that the values for the changes of the rotational constants presented in Table 1 are not only due to electronic effects, but also effectively incorporate some averaged centrifugal distortion contributions in the electronically excited state. Whereas we use ground-state rotational constants determined using a Hamiltonian in Watson's A reduction including quartic centrifugal distortion terms, we describe the vibronically excited states in an effective-rigid-rotor Hamiltonian. However, this contribution is negligible compared to the actual electronic effects.

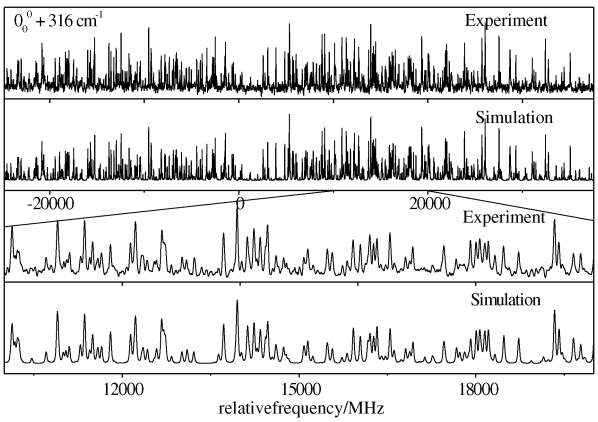

Fig. 3 Rotationally resolved spectrum of the 316 cm^{-1} band, along with a simulation of the spectrum using the best parameters from an ES fit, given in Table 1.

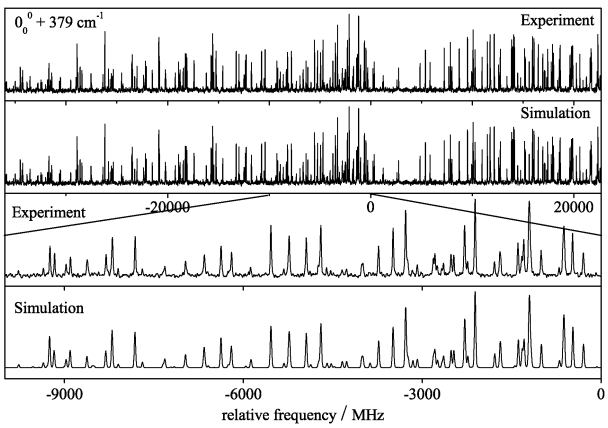

Fig. 4 Rotationally resolved spectrum of the 379 cm^{-1} band, along with a simulation of the spectrum using the best parameters from an ES fit, given in Table 1.

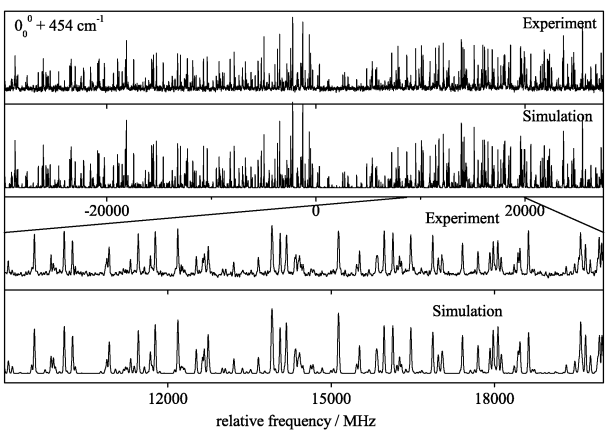

Fig. 5 Rotationally resolved spectrum of the 454 cm^{-1} band, along with a simulation of the spectrum using the best parameters from an ES fit, given in Table 1.

axis reorientation angle θ_T for excitation to ^1L_b must also be positive, also in agreement with the calculations in paper I. For the pure ^1L_a state both signs are reversed and θ_T and θ are both negative.[2]

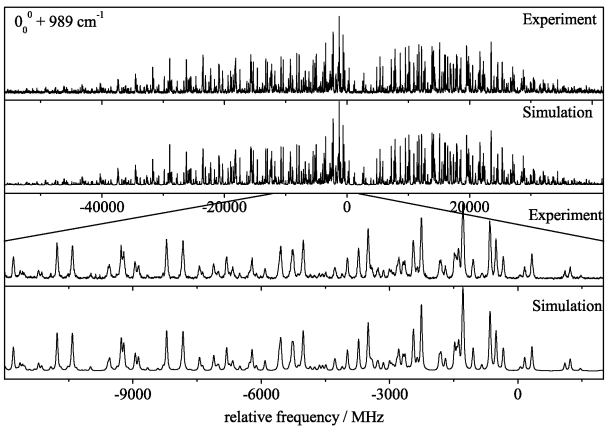

Fig. 6 Rotationally resolved spectrum of the 989 cm^{-1} band, along with a simulation of the spectrum using the best parameters from an ES fit, given in Table 1.

For the band at 316 cm^{-1} the same sign is found for both angles, and the transition moment angle is positive; thus, this band can safely be assigned as a vibrational band of the ^1L_b electronic state. The vibronic analysis given in the first paper shows that this band is the first overtone of the lowest out-of-plane vibration (42_0^2).[2]

The bands at 379 and 539 cm^{-1} were previously assigned to the in-plane vibrational modes 29 and 27, respectively.[16] This assignment is strongly supported by the vibronic analysis of paper I.[2] They both have very small TDM angles, *i.e.*, show an intermediate behavior between ^1L_a and ^1L_b with respect to their electronic nature. Assignment of these bands to a specific electronic state needs to be deferred for further discussion (*vide infra*).

The first band with a clear ^1L_a signature is the one at 454 cm^{-1}. This band was initially assigned to the lower component of a split origin of the ^1L_a state,[15] but later Barstis *et al.*[16] assigned the 454 cm^{-1} band to a combination band of two out-of-plane vibrations, 39 and 41. The vibronic analysis given in the first paper reassigns this band to the $40_0^1 41_0^1$ combination band. We find opposite signs of θ and θ_T for this band. Since the sign and magnitude of θ_T are determined geometrically, it can safely be assumed that it must have the same sign as the electronic origin. Under this assumption, the sign of θ must be reversed, yielding an absolute value of -32°, close to the theoretically predicted value of -37° for ^1L_a-transitions from the DFT/MRCI calculations of paper I. This band represents the lower component of a Fermi diad with the in-plane vibration 28. The higher component of this Fermi diad at 480 cm^{-1} also exhibits a clear ^1L_a signature as deduced from the relative signs of θ and θ_T, with a larger value of $\theta = -46^\circ$ that is also in good agreement with the theoretically predicted value. The ^1L_a signature of the 454 cm^{-1} band is apparently mediated through the Fermi resonance with the strongly vibronically coupled band at 480 cm^{-1}.

The transition at 718 cm^{-1} (mode 26), is assigned to the ^1L_b state based on the relative signs of θ and θ_T, in agreement with the previous assignment by Sammeth *et al.*[15] based on two-photon spectroscopy. The 720 cm^{-1} band ($29_0^1 41_0^2$) is also assigned as ^1L_b band from the TDM orientation, in agreement with the results of the two-photon spectra.[15]

Table 1 Molecular parameters for the excited vibronic states from fits to the rotationally resolved spectra of thirteen vibronic transitions of indole; all transitions start in the vibronic ground state whose parameters are well-known.[3,4] The derived excited state parameters are the changes of the rotational constants ΔA, ΔB, ΔC (defined as $\Delta X = X' - X''$) upon excitation, the inertial defects $\Delta I'$, the transition dipole-moment-orientation angles θ, the axis-reorientation angles θ_T, the lifetimes τ, and the vibronic-origin wavenumbers $\tilde{\nu}_0$ and $\Delta\tilde{\nu}_0$. For the vibrational assignments, see the text

Rel. wavenumber	0	+316	+379	+454	+480	+539	+718	+720	+736	+907	+908	+968	+989
Vib. assignment	0	42_0^2	29_0^1	$40_0^1 41_0^1$	28_0^1	27_0^1	26_0^1	$29_0^1 41_0^2$	$41_0^1 37_0^1$	$27_0^1 41_0^2$	23_0^1	$28_0^1 40_0^2$	$38_0^1 40_0^2 41_0^1$
ΔA/MHz	−134.82(1)	−152.30(2)	−127.56(2)	−135.16(1)	−133.84(3)	−134.47(2)	−137.61(2)	−138.89(16)	−141.72(1)	−138.24(3)	−138.82(4)	−135.04(2)	−136.24(1)
ΔB/MHz	−17.89(1)	−14.45(1)	−16.12(2)	−18.03(1)	−17.35(2)	−17.74(2)	−17.79(3)	−16.32(8)	−20.14(1)	−17.51(2)	−18.57(2)	−16.47(2)	−18.56(1)
ΔC/MHz	−20.74(1)	−17.93(1)	−20.90(1)	−19.19(1)	−21.43(2)	−19.98(1)	−20.37(1)	−19.43(4)	−19.49(1)	−19.53(1)	−19.26(1)	−20.18(2)	−20.64(1)
$\Delta I'$/uÅ^2	−0.152(2)	−1.241(2)	+0.523(6)	−0.827(9)	+0.232(9)	−0.405(6)	−0.390(4)	+0.524(4)	−1.341(5)	−0.691(5)	−1.019	−1.364(9)	−1.347(5)
θ/°	±38.9(1)	±52.8(1)	±5(2)	±32.06(3)	±46.36(3)	±8.0(3)	±47.(5)	±45.3(7)	±45.05(4)	±48.9(3)	±39.7(5)	±31.7(2)	± 24.28(5)
θ_T/°	±0.40(3)	±0.20(7)	0	∓0.08(4)	∓0.65(1)	0	±0.7(3)	±0.14(3)	±0.82(1)	±0.23	∓0.96	±0.4(1)	± 0.61(2)
τ/ns	17.6(1)	7.3(1)	16.3(3)	16.4(4)	8.4(1)	5.0(2)	4.3(9)	4.9(5)	5.2(2)	4.1(10)	4.1(10)	3.2(2)	4.8(2)
$\tilde{\nu}_0$/cm^{-1}	35231.42(1)	35546.97(1)	35610.79(1)	35685.62(1)	35711.11(1)	35770.84(1)	35949.00(1)	35951.02(1)	35967.61(1)	36138.59(1)	36139.35(1)	36199.70(1)	36220.38(1)
$\Delta\tilde{\nu}_0$/cm^{-1}	0	315.55(1)	379.36(1)	454.21(1)	479.69(1)	539.42(1)	717.58(1)	719.60(1)	736.19(1)	907.17(1)	907.93(1)	968.28(1)	988.96(1)

Also the four bands at 736, 907, 968, and 989 cm^{-1} above the origin, can be assigned to belong to the ^1L_b state based on the relative orientation of their θ and θ_T values.

The highest-wavenumber band with electronic ^1L_a character we have found so far is located at 908 cm^{-1} above the origin and is assigned to the in-plane mode 23 based on comparison to the calculated values in Tables 5 and 6 in the first paper.[2] In agreement with this, we found strong HT activity in this mode from the FCHT analysis.

5.2 Inertial defects

Further guidance in the assignment of vibronic bands can be obtained from the inertial defects and from the changes of the rotational constants upon vibronic excitation. The inertial defect is defined as $\Delta I = I_c - I_b - I_a$ and is composed of vibrational, centrifugal and electronic contributions.[37] For planar molecules it is expected to be close to zero, with out-of-plane vibrations generally causing a negative contribution to the inertial defect, and in-plane vibrations often having a small positive contribution.[38]

The experimental inertial defect of the vibronic ground state of indole is determined from microwave rotational constants[3,4] to be −0.11146 uÅ^2, a value typical for a medium-size planar aromatic molecule with low frequency out-of-plane vibrations.[39]

However, some of the excited vibronic states investigated show large positive inertial defects, as shown in Table 1. Since such large positive inertial defects are rarely found in the literature, we further investigated this effect. An anharmonic analysis of the vibrational spectrum allows, in principle, for the determination of vibrational averaging effects due to the individual vibrational motion.[40] Such an anharmonic analysis is implemented in the Gaussian program package.[41] Since the procedure for the calculation of cubic and of some of the quartic force constants needs third derivatives of the potential energy with respect to the normal coordinates, the method can currently only be applied to electronic ground-state molecules for which analytical second derivatives are available. A corresponding analysis for excited states, using solely numerical derivatives, would be prohibitively time-consuming and of very low accuracy.

Nevertheless, a good estimate of the vibrational effects in an electronically excited ^1L_b state can be provided by a vibrational analysis of the electronic ground state S_0. This assumes that the direction and amplitude of the vibrational displacement vectors is similar in the ground and the electronically excited states; see Table 5 of paper I for a comparison. The change of the rotational constants upon vibronic excitation can then be assessed from the sum of the zero-point averaged changes due to pure electronic excitation and to changes due to the individual vibrational excitation. The former are experimentally obtained from the changes of the rotational constants of the vibrationless origin, the latter from the vibrational anharmonic analysis. However, this analysis is not accurate enough to provide information on states with more than two quanta of vibrational excitation and, therefore, these bands are omitted from the analysis. Table 2 shows the resulting inertial defects of the individual vibronic states, the

Table 2 Inertial defects of the excited vibronic states $\Delta I'$, vibrational contributions to the rotational constants of the excited vibronic states A'_{vib}, B'_{vib}, C'_{vib}, (defined as $X_{vib}(Q_i) = X(Q_i) - X(Q_0)$), and changes of the rotational constants upon vibronic excitation ΔA, ΔB, and ΔC (defined as $\Delta X = X' - X''$). Experimental values are extracted from the parameters in Table 1, calculated values are from an anharmonic analysis of the electronic ground state at the MP2/6311G(d,p) level of theory; see text for details

Vibration	0	42_0^2	29_0^1	$40_0^1 41_0^1$	28_0^1	27_0^1	26_0^1	23_0^1	$41_0^1 37_0^1$
	Exp./calc.	Exp./calc.	Exp./calc.	Exp./calc.	Exp./calc.	Exp./calc.	Exp./calc.	Exp./calc.	Exp./calc.
$\Delta I'$/uÅ^2	−0.15/−0.17	−1.24/−1.17	0.52/0.37	−0.83/−0.89	0.23/0.56	−0.40/−0.33	−0.39/−0.10	−1.019/+0.05	−1.34/−1.00
A'_{vib}/MHz	0/0	−17.48/−17.03	7.26/8.60	−0.34/0.39	0.98/3.21	0.35/1.92	−2.79/−2.40	−4.00/−3.06	−6.90/−3.96
ΔA/MHz	−134.82/−134.82	−152.30/−151.85	−127.56/−126.22	−135.16/−134.43	−133.84/−131.61	−134.47/−132.90	−137.61/−137.22	−138.82/−137.88	−2.25/−0.60
B'_{vib}/MHz	0/0	3.44/2.25	1.77/0.99	−0.20/−0.36	0.54/0.36	0.15/0.18	0.17/−0.75	−0.68/0.36	1.25/1.50
ΔB/MHz	−17.89/−17.89	−14.45/−15.64	−16.12/−16.90	−18.09/−18.25	−17.35/−17.53	−17.74/−17.70	−17.72/−18.64	−18.57/−17.53	−141.72/−138.78
C'_{vib}/MHz	0/0	2.81/2.19	−0.16/−0.15	1.55/1.71	−0.69/−1.44	0.76/0.66	0.40/−0.78	−1.34/−0.66	−20.14/−18.49
ΔC/MHz	−20.74/−20.74	−17.93/−18.55	−20.90/−20.89	−19.19/−19.03	−21.43/−22.18	−19.98/−20.08	−20.34/−21.52	−19.26/−21.40	−19.49/−19.24

vibrational contributions to the rotational constants, and the changes of rotational constants upon vibronic excitation.

This vibrational analysis even allows for distinction of different vibronic bands through the changes of the rotational constants. The vibrational contribution of the 42_0^2 vibration to A rotational constant is approximately −17 MHz, while for the 29_0^1 band a value of 8 MHz is found. From these values changes of A (and also the respective changes of B and C) upon vibronic excitation are obtained, that are in good agreement with the experimental ones.

With this data in hand, we can further investigate the individual vibronic states. The 316 cm^{-1} band shows a large negative inertial defect (see Table 1), in agreement with its previous assignment as the first overtone of the out-of-plane vibration 42.[13] The 379 cm^{-1} band, which has been assigned to the in-plane 29_0^1 vibration, shows a large and positive inertial defect upon electronic excitation in theory and experimentally, nicely confirming this assignment.

The large negative inertial defect of the 454 cm^{-1} band ($40_0^1 41_0^1$) supports its assignment as an out-of-plane vibration.[13] The reassignment of this band on the basis of the vibronic analysis given in paper I[2] is fully confirmed by the calculated inertial defects and by the changes of the rotational constants in Table 2. No other calculated combination band or overtone band in the appropriate frequency range has vibrational contributions, that are closer to the experimental ones than the $40_0^1 41_0^1$ combination band. This band represents the lower component of a Fermi diad with the in-plane vibration 28 at 480 cm^{-1} being the higher component. For the 28_0^1 band, the change of the inertial defect is again large and positive, similar to the 29_0^1 band. Again, the vibrational analysis gives the correct sign and magnitude of ΔI and also the changes of the rotational constants are in close agreement with the experimental ones.

The vibronic bands at 539 (27_0^1) and 718 cm^{-1} (26_0^1) show slightly negative inertial defects. From Table 2 it can be inferred that both bands are in-plane vibrations. The calculated and observed inertial defects and rotational constant changes are in good agreement. This demonstrates, that vibrational averaging of in-plane vibrations also might lead to negative inertial defects.

The large negative inertial defect of the vibronic band at 736 cm^{-1} confirms its out-of-plane character. It was previously assigned as the first overtone of mode 38.[16] Nevertheless, the vibrational analysis shows that the combination band $41_0^1 37_0^1$ fits both the inertial defect and the changes of the rotational constants, much better than the overtone 38_0^2. We therefore reassign this vibronic band accordingly.

The band at 908 cm^{-1} shows a strong negative inertial defect which is not reproduced by the theoretical description of the assigned mode 23. Since this mode shows strong Duschinksy activity, we tentatively ascribe the mismatch to the poor description of the excited-state mode by the ground-state model.

Although no computational analysis is available for the bands at 720, 907, 968, and 989 cm^{-1} (*vide supra*), the experimental data given in Table 1 provides detailed information. The band at 720 cm^{-1}, assigned as $29_0^1 41_0^2$, shows a large positive inertial defect, which can be attributed to its in-plane 29_0^1 component, which also has a large positive inertial defect.

The bands at 907 cm^{-1}, 968 cm^{-1}, and 989 cm^{-1}, tentatively assigned to $27_0^1 41_0^2$, $28_0^1 40_0^2$, and $38_0^1 40_0^2 41_0^1$, respectively, again show strongly negative ΔIs as a consequence of their out-of-plane character.

5.3 Natural lifetimes

The natural lifetime of the ^1L_b state is determined to be 17.5 ns from the origin band, in agreement with previous time-resolved[10,13] and high-resolution-spectroscopic studies.[6] The lifetimes of all vibrationally excited states are shorter, varying between 3 and 16 ns. However, for higher vibrational states, there are discrepancies between previous time-resolved studies[13] and our data. We have carefully checked our results and are confident that they are correct to within the specified standard deviations. Generally, we find that the lifetime decreases monotonically with the excitation energy, *cf.* Table 1, which is in agreement with previous studies.[13] However, this is not true for the band at 316 cm^{-1}, for which the lifetime is especially short (7 ns) compared to the following bands (15 ns). In the first paper, we showed, that the ^1L_b state is coupled vibronically to the $\pi\sigma^*$ state *via* out-of-plane vibrations. It therefore stands to reason, that the coupling to a repulsive electronic state reduces the radiative lifetime of the coupling mode considerably. The lifetimes of the bands at 480 and 539 cm^{-1} are also significantly shorter than those of energetically lower bands. The band at 968 cm^{-1} has τ = 3.2 ns and shows the shortest lifetime of all investigated states. Therefore, we conclude that the lifetimes clearly show vibronic ^1L_b–^1L_a coupling for the bands at 316, 480, 539, and 968 cm^{-1} and hint at weak coupling for the bands at 379 and 454 cm^{-1}. Regarding the vibronic coupling, the lifetimes provide no further insight into the bands at 718, 720, 736, 907, 908, and 989 cm^{-1}, all of which have short lifetimes of approximately 4–5 ns.

5.4 Comparison with the theoretical analysis from paper I

The first comparison of the experimental results we make is with regard to the calculated structures. We obtained the CC2 structure for the electronic ground state and for the excited ^1L_a and ^1L_b states. Only the changes of the rotational constants for excitation to the ^1L_b state match the experimentally determined changes for each of the investigated bands. Thus, from purely structural considerations, direct excitation of ^1L_a bands in the investigated range can be excluded.

From the *ab initio* optimized structures, the angle of axis reorientation upon electronic excitation could be determined. We found for the ^1L_b state that both the axis reorientation angle θ_T as well as the angle of the transition dipole with the inertial *a*-axis θ are positive. For the ^1L_a state both angles were found to be negative. No change of sign between θ and θ_T was found in the calculations for the zero-order ^1L_a and ^1L_b states. Nevertheless, in the experiment, we found bands with alternating signs for θ and θ_T, showing the importance of vibronic coupling of the two states for the interpretation of the spectra.

From the discussion of the experimental results, we deduce vibronic ^1L_b–^1L_a coupling for the bands at 316, 379, 454, 480, 539, 720, 910, and 968 cm^{-1}. The coupling is especially evident, with very strong effects in more than one of the criteria discussed above, for the bands at 379, 480, and 539 cm^{-1}. This is in very good agreement with the theoretical description in paper I. We assign the three strongly coupled bands to the modes 29 (379 cm^{-1}), 28 (480 cm^{-1}), and 27 (539 cm^{-1}) from the theoretical analysis in paper I. In the calculations these bands all show strong HT coupling ($|HT| \geq 0.05$), supporting their experimental ^1L_a character. Moreover, mode 28 (480 cm^{-1}) is the lowest fundamental with a clear ^1L_a TDM orientation in the theoretical and in the experimental results.

However, the 454 cm^{-1} band is the lowest wavenumber vibration for which the Herzberg–Teller analysis from paper I predicts a negative angle between the *a*-axis and the TDM, giving further evidence for the assignment of this band as being due to vibronic coupling to the ^1L_a state. Nevertheless, the experimentally determined long lifetime and the weak calculated HT coupling both support the previous argument that this band gains ^1L_a character only indirectly through the Fermi resonance with the band at 480 cm^{-1}.

In the experimental analysis the band at 316 cm^{-1} (mode 42) has a regular TDM and a regular inertial defect for an out-of-plane vibration. Moreover, from paper I it is also evident that it shows only a small HT coupling strength. This coupling must be to a state of out-of-plane symmetry and therefore cannot be the ^1L_a state. Instead, it might be the $\pi\sigma^*$ state, whose repulsive character would then give a logical explanation for its short lifetime.

The 720 cm^{-1} band is a combination of mode 29 and the overtone of mode 41. This is in agreement with the fact that it has a somewhat reduced (*i.e.*, the reduced positive inertial defect change) but nevertheless clear ^1L_a character compared to the 379 cm^{-1} band (mode 29). The same holds for the 968 cm^{-1} band (combination of mode 28 and the overtone of mode 40) with respect to the 480 cm^{-1} band (mode 28). In summary, it is clear from experiment and theory that these two bands are strongly HT coupled to ^1L_a.

The band at 907 cm^{-1} does not show clear signs of vibronic coupling to the ^1L_a state, although it is a combination mode involving mode 27, which itself (539 cm^{-1}) is clearly vibronically coupled to the ^1L_a state.

Besides the origin, the bands at 718, 736, and 989 cm^{-1} show no sign of ^1L_a character. Based on the vibrational frequencies and the TDMs we assign these bands to the modes 26, a combination of 37 and 41, and a combination band of mode 38, mode 41 and the overtone of mode 40, respectively. Therefore, the bands at 736 and 989 cm^{-1} ($37_0^1 41_0^1$ and $38_0^1 40_0^2 41_0^1$) are barely vibronically coupled to the ^1L_a state in the calculations. The 718 cm^{-1} band (mode 26), however, has nearly equal FC and HT strength. Nevertheless, this mode assignment, together with Table 6 from ref. 2, can also be exploited to determine the as-of-yet undecided sign of the TDM of this band to be $+45°$, very similar to the ^1L_b origin value.

6. Conclusions

We have recorded and analyzed thirteen vibronic bands of indole from the electronic origin up to 989 cm^{-1} above,

yielding accurate vibrational shifts, inertial parameters, axis reorientation angles upon excitation, transition-dipole-moment orientations, inertial defect changes, and excited state lifetimes. These experimental results are compared to the computational description presented in paper I and fully support that theoretical analysis on the basis of ^1L_b–^1L_a Herzberg–Teller coupling. We demonstrate that the changes of the rotational constants upon vibronic excitation and the respective inertial defects of the vibronic states contain sufficient information about the vibrational modes to be used as a—typically overlooked—tool for vibrational assignments.

For the electronic origin band our analysis supports previous assignments as an ^1L_b transition. Nevertheless, six bands, out of the eleven bands recorded and analyzed, show ^1L_a character. These are most notably the three lowest-wavenumber in-plane vibrations at 379, 480, and 539 cm^{-1}. The bands at 720 and 968 cm^{-1} are combination bands containing one of these strongly coupled fundamentals and, therefore, obtain their ^1L_a character through these coupled fundamentals. The band at 454 cm^{-1} gains its ^1L_a character through a Fermi resonance with the strongly coupled 480 cm^{-1} band.

Overall, the combined theoretical and experimental investigation presented here and in the preceding paper provide a clear picture of the ^1L_b and ^1L_a electronic states of indole and the vibronic coupling between them. The ^1L_a state is located more than 1000 cm^{-1} above the ^1L_b state. The general quality of the theoretical description[2] suggests that the predicted ^1L_a–^1L_b separation of 1850 cm^{-1} provides a good estimate of the energetic location of the ^1L_a electronic state. However, it is also clear that the electronic properties of the indole chromophore, for example, the transition-dipole-moment orientation in the molecular frame, are a mixture of ^1L_b and ^1L_a character through Herzberg–Teller coupling already a few hundred wavenumbers above the electronic origin of the ^1L_b state. Specific vibrations are more effective at producing this coupling than others.

As stated in the preceding publication we cannot rule out, that coupling of the ^1L_b state occurs as well to higher lying electronic states like the B_b and B_a in Platt's notation. Although they are energetically far away, they might show coupling to some extent, due to large transition dipole moments. Nevertheless, none of our conclusions critically depends on the assumption, that coupling is mediated by a single electronic state.

A second Herzberg–Teller coupling between the ^1L_b state and the energetically higher lying $\pi\sigma^*$ state, mediated through the out-of-plane vibrations is suggested from the theoretical results in paper I and from the short lifetime of the out-of-plane mode 42. Since the $\pi\sigma^*$ state is repulsive, a vibrational motion directed towards the coupling state may lower the effective barrier, formed *via* a conical intersection of the ^1L_b and the $\pi\sigma^*$, thus facilitating tunneling through this barrier. This mechanism could explain the exceptionally short lifetime of the overtone of the out-of-plane band 42.

It is clear from the data presented here that high resolution-spectroscopy, examining "static"—or time-averaged—molecular properties, can provide detailed access to the dynamics in the electronically excited states of indole. This includes the conical intersection of the bound ^1L_b and ^1L_a states. This can be understood from the fact that molecular eigenstates are formed from linear combinations of zero-order ^1L_b and ^1L_a states, and that the vibrational motion of these eigenstates senses the complete populated configurational phase-space, according to the probability density of its wavefunction. Since the overall rotations are slow compared to the vibrations, one obtains vibrationally averaged rotational constants, which reflect these dynamical aspects of the observed coupling.

Acknowledgements

We thank Wayne E. Sinclair for expert help in the early stage of the experiments. This work was supported by the Deutsche Forschungsgemeinschaft (DFG) in the framework of the NWO-DFG bilateral program (SCHM1043/10-1), by the Netherlands Organization for Scientific Research (NWO), and by NSF (CHE-0911117). We acknowledge the National Computer Facilities of NWO for a grant on the Netherlands supercomputing facility SARA.

References

1 J. T. Vivian and P. R. Callis, *Biophys. J.*, 2001, **80**, 2093.
2 C. Brand, J. Küpper, D. W. Pratt, W. L. Meerts, D. Krügler, J. Tatchen and M. Schmitt, *Phys. Chem. Chem. Phys.*, 2010, DOI: 10.1039/c001776k.
3 R. D. Suenram, F. J. Lovas and G. T. Fraser, *J. Mol. Spectrosc.*, 1988, **127**, 472.
4 W. Caminati and S. di Bernardo, *J. Mol. Struct.*, 1990, **240**, 253.
5 L. A. Philips and D. H. Levy, *J. Chem. Phys.*, 1986, **85**, 1327.
6 G. Berden, W. L. Meerts and E. Jalviste, *J. Chem. Phys.*, 1995, **103**, 9596.
7 C. Kang, T. M. Korter and D. W. Pratt, *J. Chem. Phys.*, 2005, **122**, 174301.
8 J. R. Platt, *J. Chem. Phys.*, 1949, **17**, 484.
9 Y. Yamamoto and J. Tanaka, *Bull. Chem. Soc. Jpn.*, 1972, **45**, 1362.
10 J. W. Hager and S. C. Wallace, *J. Phys. Chem.*, 1983, **87**, 2121.
11 J. Zuclich, J. U. von Schütz and A. H. Maki, *J. Am. Chem. Soc.*, 1974, **96**(3), 710.
12 B. J. Fender, K. W. Short, D. K. Hahn and P. R. Callis, *Int. J. Quantum Chem.*, 1999, **72**, 347.
13 G. A. Bickel, D. R. Demmer, E. A. Outhouse and S. C. Wallace, *J. Chem. Phys.*, 1989, **91**, 6013.
14 B. Albinsson and B. Nordén, *J. Phys. Chem.*, 1992, **96**, 6204.
15 D. M. Sammeth, S. Yan, L. H. Spangler and P. R. Callis, *J. Phys. Chem.*, 1990, **94**, 7340.
16 T. L. O. Barstis, L. I. Grace, T. M. Dunn and D. L. Lubman, *J. Phys. Chem.*, 1993, **97**, 5820.
17 B. J. Fender, D. M. Sammeth and P. R. Callis, *Chem. Phys. Lett.*, 1995, **239**, 31.
18 J. W. Hager and S. C. Wallace, *J. Phys. Chem.*, 1984, **88**, 5513.
19 M. J. Tubergen and D. H. Levy, *J. Phys. Chem.*, 1991, **95**, 2175.
20 J. R. Carney, F. C. Hagemeister and T. S. Zwier, *J. Chem. Phys.*, 1998, **108**, 3379.
21 K. W. Short and P. R. Callis, *J. Chem. Phys.*, 1998, **108**, 10189.
22 T. M. Korter, D. W. Pratt and J. Küpper, *J. Phys. Chem. A*, 1998, **102**, 7211.
23 R. M. Helm, M. Clara, T. L. Grebner and H. J. Neusser, *J. Phys. Chem. A*, 1998, **102**, 3268.
24 T. M. Korter, J. Küpper and D. W. Pratt, *J. Chem. Phys.*, 1999, **111**, 3946.
25 W. A. Majewski, D. F. Plusquellic and D. W. Pratt, *J. Chem. Phys.*, 1989, **90**, 1362.
26 M. Schmitt, J. Küpper, D. Spangenberg and A. Westphal, *Chem. Phys.*, 2000, **254**, 349.
27 S. Gerstenkorn and P. Luc, *Atlas du spectre d'absorption de la molécule d'iode 14 800–20 000 cm^{-1}*, CNRS, Paris, 1986.

28 A. Ostermeier, A. Gawelczyk and N. Hansen, *Lecture Notes in Computer Science: Parallel Problem Solving from Nature (PPSN III)*, Springer, 1994, pp. 189–198.
29 J. Küpper, *Rotationsauflösende Laserspektroskopie-Beziehung zwischen Struktur und interner Dynamik von Molekülen*, PhD thesis, Heinrich-Heine-Universität, Math. Nat. Fakultät, Düsseldorf, 2000.
30 O. M. Shir and T. Bäck, in *GECCO '07: Proceedings of the 9th Annual Conference on Genetic and Evolutionary Computation*, ACM, New York, NY, USA, 2007, pp. 713–721.
31 I. Kalkman, C. Vu, M. Schmitt and W. L. Meerts, *ChemPhysChem*, 2008, **9**, 1788.
32 W. L. Meerts, M. Schmitt and G. Groenenboom, *Can. J. Chem.*, 2004, **82**, 804.
33 W. L. Meerts and M. Schmitt, *Phys. Scr.*, 2006, **73**, C47.
34 W. L. Meerts and M. Schmitt, *Int. Rev. Phys. Chem.*, 2006, **25**, 353.
35 J. A. Hageman, R. Wehrens, R. de Gelder, W. L. Meerts and L. M. C. Buydens, *J. Chem. Phys.*, 2000, **113**, 7955.
36 A. Held, B. B. Champagne and D. W. Pratt, *J. Chem. Phys.*, 1991, **95**, 8732.
37 T. Oka and Y. Morino, *J. Mol. Spectrosc.*, 1961, **6**, 472.
38 W. Gordy and R. L. Cook, *Microwave Molecular Spectra*, Wiley, New York, 3rd edn, 1984.
39 T. Oka, *J. Mol. Struct.*, 1995, **352–353**, 225.
40 V. Barone, *J. Chem. Phys.*, 2005, **122**, 014108.
41 M. J. Frisch, G. W. Trucks, H. B. Schlegel, G. E. Scuseria, M. A. Robb, J. R. Cheeseman, J. A. Montgomery, Jr., T. Vreven, K. N. Kudin, J. C. Burant, J. M. Millam, S. S. Iyengar, J. Tomasi, V. Barone, B. Mennucci, M. Cossi, G. Scalmani, N. Rega, G. A. Petersson, H. Nakatsuji, M. Hada, M. Ehara, K. Toyota, R. Fukuda, J. Hasegawa, M. Ishida, T. Nakajima, Y. Honda, O. Kitao, H. Nakai, M. Klene, X. Li, J. E. Knox, H. P. Hratchian, J. B. Cross, C. Adamo, J. Jaramillo, R. Gomperts, R. E. Stratmann, O. Yazyev, A. J. Austin, R. Cammi, C. Pomelli, J. W. Ochterski, P. Y. Ayala, K. Morokuma, G. A. Voth, P. Salvador, J. J. Dannenberg, V. G. Zakrzewski, S. Dapprich, A. D. Daniels, M. C. Strain, O. Farkas, D. K. Malick, A. D. Rabuck, K. Raghavachari, J. B. Foresman, J. V. Ortiz, Q. Cui, A. G. Baboul, S. Clifford, J. Cioslowski, B. B. Stefanov, G. Liu, A. Liashenko, P. Piskorz, I. Komaromi, R. L. Martin, D. J. Fox, T. Keith, M. A. Al-Laham, C. Y. Peng, A. Nanayakkara, M. Challacombe, P. M. W. Gill, B. Johnson, W. Chen, M. W. Wong, C. Gonzalez and J. A. Pople, *GAUSSIAN 03, revision a.1*, Gaussian, Inc., Pittsburgh, PA, 2003.

